Early Last Interglacial ocean warming drove substantial ice mass loss from Antarctica

Authors

Chris S.M. Turney, Christopher J. Fogwill, Nicholas R. Golledge, Nicholas P. McKay, Erik van Sebille, Richard T. Jones, David Etheridge, Mauro Rubino, David P. Thornton, Siwan M. Davies, Christopher Bronk Ramsey, Zoë Thomas, Michael I. Bird, Niels C. Munksgaard, Mika Kohno, John Woodward, Kate Winter, Laura S. Weyrich, Camilla M. Rootes, Helen Millman, Paul G. Albert, Andres Rivera, Tas van Ommen, Mark Curran, Andrew Moy, Stefan Rahmstorf, Kenji Kawamura, Claus-Dieter Hillenbrand, Michael E. Weber, Christina J. Manning, Jennifer Young and Alan Cooper

Early Last Interglacial ocean warming drove substantial ice mass loss from Antarctica

Authors

Chris S.M. Turney[1,2,3*], Christopher J. Fogwill[1,2,4], Nicholas R. Golledge[5,6], Nicholas P. McKay[7], Erik van Sebille[2,8,9], Richard T. Jones[10]†, David Etheridge[11], Mauro Rubino[4], David P. Thornton[11], Siwan M. Davies[12], Christopher Bronk Ramsey[13], Zoë Thomas[1,2,3], Michael I. Bird[14,15], Niels C. Munksgaard[15,16], Mika Kohno[17], John Woodward[18], Kate Winter[18], Laura S. Weyrich[19,20], Camilla M. Rootes[21], Helen Millman[2], Paul G. Albert[13], Andres Rivera[22], Tas van Ommen[23,24], Mark Curran[23,24], Andrew Moy[23,24], Stefan Rahmstorf[25,26], Kenji Kawamura[27,28,29] Claus-Dieter Hillenbrand[30], Michael E. Weber[31], Christina J. Manning[32], Jennifer Young[19,20] and Alan Cooper[19,20]

Affiliations

1. Palaeontology, Geobiology and Earth Archives Research Centre, School of Biological, Earth and Environmental Sciences, University of New South Wales, Australia

2. Climate Change Research Centre, School of Biological, Earth and Environmental Sciences, University of New South Wales, Australia

3. ARC Centre of Excellence in Australian Biodiversity and Heritage, School of Biological, Earth and Environmental Sciences, University of New South Wales, Australia

4. School of Geography, Geology and the Environment, Keele University, ST5 5BG, UK

5. Antarctic Research Centre, Victoria University of Wellington, Wellington 6140,

New Zealand

6. GNS Science, Avalon, Lower Hutt, New Zealand

7. School of Earth and Sustainability, Northern Arizona University, Flagstaff, Arizona 86011, USA

8. Grantham Institute & Department of Physics, Imperial College London, London, UK

9. Institute for Marine and Atmospheric Research Utrecht, Utrecht University, Utrecht, Netherlands

10. Department of Geography, Exeter University, Devon, EX4 4RJ, UK

11. Climate Science Centre, CSIRO Ocean and Atmosphere, Aspendale, Victoria, 3195 Australia

12. Department of Geography, Swansea University, Swansea, UK

13. Research Laboratory for Archaeology and the History of Art, University of Oxford, Dyson Perrins Building, South Parks Road, Oxford, OX1 3QY, UK

14. Centre for Tropical Environmental and Sustainability Science, College of Science and Engineering, James Cook University, Cairns, Australia

15. ARC Centre of Excellence in Australian Biodiversity and Heritage, James Cook University, Cairns, Australia

16. Research Institute for the Environment and Livelihoods, Charles Darwin University, Australia

17. Department of Geochemistry, Geoscience Center, University of Göttingen, Goldschmidtstr. 1, 37077 Göttingen, Germany

18. Department of Geography and Environmental Sciences, Faculty of Engineering and Environment, Northumbria University, Newcastle upon Tyne, NE1 8ST, UK

19. Australian Centre for Ancient DNA, University of Adelaide, Australia

20. ARC Centre of Excellence in Australian Biodiversity and Heritage, University of Adelaide, Australia

21. Department of Geography, University of Sheffield, UK

22. Glaciology and Climate Change Laboratory, Centro de Estudios Cientficos, Valdivia, Arturo Prat 514, Chile

23. Department of the Environment and Energy, Australian Antarctic Division, 203 Channel Highway, Kingston, Tasmania 7050, Australia

24. Antarctic Climate & Ecosystems Cooperative Research Centre, University of Tasmania, Private Bag 80, Hobart, Tasmania 7001, Australia

25. Potsdam Institute for Climate Impact Research (PIK), PO Box 60 12 03, D-14412 Potsdam, Germany.

26. University of Potsdam, Institute of Physics and Astronomy, Germany.

27. National Institute of Polar Research, Research Organizations of Information and Systems, 10-3 Midori-cho, Tachikawa, Tokyo 190-8518, Japan

28. Department of Polar Science, Graduate University for Advanced Studies (SOKENDAI), 10-3 Midori-cho, Tachikawa, Tokyo 190-8518, Japan

29. Institute of Biogeosciences, Japan Agency for Marine-Earth Science and Technology, 2-15 Natsushima-cho, Yokosuka 237-0061, Japan

30. British Antarctic Survey, High Cross, Madingley Road, Cambridge CB3 0ET, UK

31. Steinmann-Institute, University of Bonn, Germany.

32. Department of Earth Sciences, Royal Holloway University of London, TW20 OEX, UK

†. Deceased.

*Corresponding author. E-mail: c.turney@unsw.edu.au

The future response of the Antarctic ice sheets to rising temperatures remains highly uncertain. A valuable analogue for assessing the sensitivity of Antarctica to warming is the Last Interglacial (129-116 kyr), when global sea level peaked 6 to 9 meters above present. Here we report a blue-ice record of ice-sheet and environmental change from the periphery of the marine-based West Antarctic Ice Sheet (WAIS). Constrained by a widespread volcanic horizon and supported by ancient microbial DNA analyses, we provide the first direct evidence for Last Interglacial WAIS collapse, driven by ocean warming and associated with destabilization of sub-glacial hydrates. Ice-sheet modelling supports this interpretation and suggests a 2˚C warming of the Southern Ocean over a millennia could trigger a ~3.2 meter rise in global sea levels. Our data indicate Antarctica is highly vulnerable to projected increases in ocean temperatures and may drive ice-climate feedbacks that further amplify warming.

The projected contribution of Antarctic ice sheets to twenty-first century global mean sea level (GMSL) ranges from negligible[1] to several metres[2,3]. A valuable analogue is the Last Interglacial (LIG or Marine Isotope Stage 5e in marine sediment records; 129-116 kyr)[4,5], which experienced warmer polar temperatures and higher GMSL (+6 to 9 m)[4,6,7] relative to present day[8,9], the most geographically widespread expression of high sea level during a previous warm period[4,6]. LIG sea level cannot be fully explained by Greenland Ice Sheet melt (<2 m)[8], ocean thermal expansion and melting mountain glaciers (~1 m)[4], implying substantial Antarctic mass loss[3,4,10]. Half a century ago John Mercer was the first to propose that the marine-based West Antarctic Ice Sheet (WAIS) is vulnerable to a warming Southern Ocean and may have made a significant contribution to global sea level during the LIG[5]. Recent work has further demonstrated that extensive deep, marine-based and reverse-sloped sectors of the East Antarctic Ice Sheet (EAIS) may have also contributed to higher LIG sea levels[10]. Whilst a relatively cool LIG preserved in the Mount Moulton blue ice field[11] may be explained by substantial WAIS mass loss[12], no direct physical evidence has yet been identified[4,13]. Climate estimates from model simulations provide an indirect measure of change, but typically suggest negligible warming compared to reconstructions[4,8] and when used to drive ice-sheet models are not sufficient to remove the floating ice shelves that buttress ice flow from central Antarctica[14]. In an attempt to bypass these problems, ice-sheet models have been driven by a wide range of prescribed climate scenarios; however, these suggest widely different sensitivities dependent on the physical model parameterization, with >2˚C (and in some instances >4˚C) ocean warming required for the loss of the WAIS, exceeding paleoclimate estimates[3,9,14,15].

Here we report a new high-resolution record of environmental change and ice flow dynamics from the Patriot Hills Blue Ice Area (BIA), exposed in Horseshoe Valley (Ellsworth Mountains; see Methods) (Fig. 1). Due to strong prevailing katabatic airflow, an extensive BIA (more than 1150 m across) has formed to the leeward side of the Patriot Hills, where ancient ice is drawn up from depth within Horseshoe Valley (Fig. 1). Regional airborne and detailed local ground-penetrating radar (GPR) surveys show a remarkably coherent series of dipping (24-45°) layers, broken by two discontinuities, which represent isochrons across the Patriot Hills BIA, extending thousands of metres into Horseshoe Valley. The BIA transect spans the time intervals 0-80 kyr and 130-134 kyr, constrained by analysis of trace gases and geochemically identified volcanic layers exposed across the transect which have been Bayesian age modelled against the recently compiled continuous 156 kyr global greenhouse gas time series (CO_2, CH_4, and N_2O)[16] on the AICC2012 age scale[17] (Methods). The record is located 50 km inland from the modern grounding line of the Filchner-Ronne Ice Shelf in the Weddell Sea Embayment (WSE)[18] and close to the Rutford Ice Stream, one of the largest methane hydrate reserves identified in Antarctica (total organic carbon estimated to be 21,000 petagrams, or 21×10^{18} g)[19]. Today precipitation at the site is delivered via storms originating from the South Atlantic or Weddell Sea. Horseshoe Valley is a locally-sourced compound glacier system (i.e. with negligible inflow) that is buttressed by, but ultimately coalesces with, the Institute Ice Stream via the Horseshoe Valley Trough, making the area sensitive to dynamic ice-sheet changes across the broader WSE[20]. Importantly, the Ellsworth Mountains also lie in a sector of the continent that is highly responsive to isostatic rebound under a scenario of substantial WAIS mass loss, potentially preserving ice from around the time of the LIG in small valley glaciers and higher ground areas[21].

Results

The isotopic series of δD across the Patriot Hills BIA exhibits a coherent record of relatively low values between 18 and 80 kyr, consistent with a glacial-age sequence (Fig. 2). Below these layers and at the periphery of zones of higher ice flow[18] we find an older unit of ice exposed at the surface expressed by a step change to enriched (interglacial) isotopic values (Fig 2 and S5), implying proximal warmer conditions and reduced sea ice extent[22]. Importantly, we identify a distinct tephra horizon near the boundary of this older unit of ice which, based on major and trace element geochemical fingerprinting (Supplementary Figs 9-11), is correlated to a volcanic ash from the penultimate deglaciation (Termination II) referred to as Tephra B in marine sediments on the West Antarctic continental margin[23] and identified at 1785.14 m depth in the Dome Fuji ice core where it is dated to 130.7±1.8 kyr (AICC2012 timescale)[17,22,23]. The start of the oldest section of the sequence is dated here to 134.1±2.2 kyr, consistent with modelling studies, airborne radio-echo sounding lines, and GPR profiles, which imply older ice exists at depth in the Ellsworth Mountains[18,21] (Fig. 1).

The combined tephra and trace gas analyses suggest a ~50 kyr hiatus after Termination II (130.1±1.8 kyr). Radio-echo sounding surveys across the WSE have identified a large subglacial basin comprising landforms reflecting restricted, dynamic, marine-proximal alpine glaciation, with hanging tributary valleys feeding an overdeepened Ellsworth Trough[24]. The extensive nature of the subglacial features implies substantial and repeated mass loss of the marine sections of the WAIS, with the ice margin some 200 km inland of present day[24]. However, the timing of most recent retreat is currently unknown. Whilst previous surface exposure dating in the region has suggested that the WAIS contribution to global sea level rise during warmer periods was limited to 3.3 m above present, relatively short-duration interglacial periods may have resulted in near-complete deglaciation[25], contributing to the sub-glacial landscape identified across the WSE during recent surveys[24]. Previous work has interpreted erosional features D1 and D2 in the Patriot Hills BIA to be a consequence of extensive ice surface lowering in Horseshoe Valley (up to ~500 m since the Last Glacial Maximum, 21 kyr) and more exposure of katabatic-enhancing nunataks, resulting in increased wind scour[20,26]. Whilst this scenario may explain unconformity D0, previous work has demonstrated Horseshoe Valley and the wider WSE to be highly sensitive to periods of rapid ice stream advance or retreat in the last glacial cycle and Holocene with dramatic reductions in surface elevation[20,26-28]. Furthermore, glaciological investigations assessing the impact of ice shelf loss on glaciers along the Antarctic Peninsula provides important insights, albeit on a smaller scale. The 2002 Larsen B ice shelf collapse led to many of the tributary glaciers abruptly changing from a convex to a concave profile[29], with relic ice left isolated on the upper flanks of the valleys[30]. Both scenarios are consistent with extensive grounding line retreat across the inner shelf of the Weddell Sea and associated substantial ice loss across the wider WSE[18].

The ice at Patriot Hills therefore appears to preserve a record of glacier flow in Horseshoe Valley up to the moment when the Filcher-Ronne Ice Shelf collapsed, after which the sequence likely remained isolated due to regional ice flow reconfiguration for multiple millennia; a situation that persisted until the ice surface had risen sufficiently to enable the regional iceflow to recover sometime during late MIS 5. The presence of a discrete older ice unit along the flanks of the Ellsworth Mountains[18] (Figs 1 and S2) and the subsequent inferred highly variable climate and/or sea ice extent across the wider WSE (Supplementary Figs 5 and 12) implies the preservation of ice from Marine Isotope Stage (MIS) 6/5 (Termination II) and 5/4 transitions in Horseshoe Valley. Our data provide the first direct evidence for a WAIS collapse during the LIG and supports previous suggestions that the southern polar region was a major driver of high global sea level[5,12,31], most likely at the onset of the interglacial[23,32,33].

Discussion

What could be the cause of this ice loss? Recent work has proposed that the iceberg-rafted Heinrich 11 event between 135 and 130 kyr (during Termination II) may have significantly reduced North Atlantic Deep Water (NADW) formation and shut down the Atlantic Meridional Overturning Circulation (AMOC)[34], resulting in a net heat transport to the Southern Hemisphere (the bipolar seesaw pattern of northern cooling and southern warming)[31] (Fig. 3). Under this scenario, surface cooling during Heinrich 11 increased the northern latitudinal temperature gradient and caused a southward migration of the Intertropical Convergence Zone and mid-latitude Southern Hemisphere westerly airflow[10,35]. In the Southern Ocean, the associated northward Ekman transport of cool surface waters (something akin to today; Fig. 1) would have been compensated by increased delivery of relatively warm and nutrient-rich deep Circumpolar Deep Water onto the Antarctic continental shelf[10,23,31,35], leading to enhanced thermal erosion of ice at exposed grounding lines[31,36]. The precise correlation between the Patriot Hills ice and West Antarctic marine records[23] afforded by the Termination II tephra demonstrates for the first time that the warming recorded in the BIA is coincident with a major, well-documented peak in marine temperatures and productivity around the Antarctic continent and in the Southern Ocean[23,35] (Fig. 2). Recent modelling results suggest that increased heat transport beneath the ice shelves can drive extensive grounding-line retreat, triggering substantial drawdown of Antarctic ice sheets[2,10,14], and projected to increase in the WSE during the twenty-first century[37]. The subsequent delivery of large volumes of associated freshwater into the Southern Ocean during the LIG would have reduced Antarctic Bottom Water (AABW) production, resulting in increased deepwater formation in the North Atlantic[31,38] (Fig. 3).

With Southern Ocean warming and concurrent ice-sheet retreat, the large methane reservoirs in Antarctic sedimentary basins (e.g. Rutford Ice Stream) would have become vulnerable to release[19], contributing to elevated atmospheric levels through the LIG[8,16] (Fig. 2). High-latitude open water and sea ice are rich in microbial communities, components of which may be collected by passing storms and delivered onto the ice sheet (e.g. prokaryotes, DNA), offering insights into offshore environmental processes[39,40]. To investigate environmental changes prior to and after the ice-sheet reconfiguration recorded in the Patriot Hills BIA, we applied a strict ancient DNA methodology and sequencing to provide the first description of ancient microbial species locked within the ice (Methods). Methane-utilizing microorganisms were found in three samples along the Patriot Hills transect and were absent from other samples and laboratory controls. The most striking feature of the Patriot Hills BIA genetic record was detected immediately prior to inferred ice loss, where *Methyloversatilis* microbes dominated the detectable microbial diversity (~130 kyr) (Fig. 2 and Supplementary Fig. 14). *Methyloversatilis* was only found in high abundance in this sample (with trace amounts identified at ~22 kyr). Crucially, *Methyloversatilis* species are facultative methylotrophs[41], consistent with elevated levels of CH_4 in the water column near the end of Termination II.

The inferred substantial mass loss across the WSE implies a major role for ocean warming during Termination II and the LIG. The most comprehensive published high-latitude (≥40˚S) network of quantified sea surface temperature (SST) estimates suggests an early LIG (~130 kyr) warming of 1.6±0.9˚C relative to present day[9,15], providing an upper limit on the sensitivity of Antarctic ice sheets to ocean temperatures. To investigate ice-sheet dynamics around the Patriot Hills and across Antarctica in response to a range of ocean warming scenarios (1˚-3˚C), we applied the Parallel Ice Sheet Model v.0.6.3 (Fig. 4)[2]. The pattern of circum-Antarctic ocean warming during this time period is not well-established so we assume a spatially-uniform warming pattern relative to present day temperatures. Our model time series illustrates that the majority of ice loss takes place within the first two millennia, depending on the magnitude of the forcing (Fig. 4 and Table 1). This corresponds to the time period of inferred loss of marine-based sectors of the ice sheet (Fig. 2), primarily in West Antarctica. In contrast to some whole-continent models, our simulations do not include mechanisms by which a grounded ice cliff may collapse[3], a process that produces considerably faster and greater ice margin retreat than reported here.

For the 2˚C warmer than present day scenario, our model predicts a contribution to GMSL rise of 3.2 m in the first millennium of forcing (Fig. 4). The loss of the Filchner-Ronne Ice Shelf within 200 years of warming triggers a non-linear response by removing the buttressing force that stabilises grounded ice across large parts of the WSE and the EAIS (most notably the Recovery Basin) (Fig. 5), consistent with other modelling studies[10,13,14]. Ongoing slower ice loss subsequently occurs around the margins of East Antarctica, producing a sustained contribution to sea-level rise.

Previous work has suggested that the Ellsworth Mountains would have experienced a relatively large positive isostatic adjustment (~500 m) accompanying the loss of the WAIS[21]. To investigate how an evolving ice-sheet geometry would manifest across the wider region, we extracted local ice surface and bed elevations for the WSE from the model simulation that uses a 2°C ocean warming with no atmospheric warming. Fig. 5 illustrates the sequence of events that take place as the ice sheet evolves. First, loss of the Filchner-Ronne Ice Shelf in the Weddell Sea triggers a non-linear response, removing the buttressing force that stabilises grounded ice across large parts of the WSE and the EAIS (most notably the Recovery Basin). The loss of back-stress allows for an acceleration of grounded ice and a rapid but short-lived thinning episode[21]. At the Patriot Hills, bedrock uplift of c. 30 m over this 0.2 kyr period is outpaced by a surface lowering of c. 75 m, implying a net ice-sheet thinning of around 105 m. Subsequently, regional-scale isostatic uplift elevates both the bed topography (c. 250 m) and ice-sheet surface (c. 350 m) relative to the initial configuration. The difference between these two values reflects positive net mass balance of the ice sheet here (~0.055 m/year). After around 2.5 kyr, renewed dynamic thinning of the ice sheet in the Patriot Hills leads to a rapid thinning and lowering of the ice sheet surface, at a rate exceeding regional-scale bedrock subsidence (120 m over 0.4 kyr, or 0.3 m/year, compared to c. 70 m over 3.2 kyr, or 0.022 m/year respectively) (Fig. 5). The Patriot Hills record is consistent with the loss of grounded ice early in the LIG[21] as a consequence of regional ice dynamic changes and isostatically-driven isolation of Horseshoe Valley from sustained ocean forcing. For the 1˚ and 3˚ warming scenarios, similar spatial losses are modelled, with GMSL rises of 1.8 and 4.0 m for the first millennium, respectively (Table 1). Atmospheric warming of the magnitude suggested in Antarctic cores (>4˚C)[11,12,42-44] adds an additional metre of equivalent global sea level within the first millennium (Supplementary Fig. 16). Whilst some modelling studies have argued the loss of the Filchner–Ronne Ice Shelf does not display a strong marine ice sheet instability feedback[45], our results suggest otherwise. The ice sheet modelling outputs supports our interpretation of the Patriot Hill BIA record, demonstrating the substantial ice-sheet flow reconfiguration and resultant isostatic response that would occur under such a scenario (Fig. 5).

The evidence for substantial mass loss from Antarctica in the early LIG has important implications for the future[4,32]. Our field-based reconstruction and modelling results support a growing body of evidence that the Antarctic ice sheets are highly sensitive to ocean temperatures. Driven by enhanced basal melt through increased heat transport into cavities beneath the ice shelves[2,36], this process is projected to increase with a weakening AMOC during the twenty-first century[37,46,47], and one which may lead to other positive feedbacks such as destabilization of methane hydrate reserves[19].

Acknowledgements

CSMT, CJF, MIB, AC and NRG are supported by their respective Australian Research Council (ARC) and Royal Society of New Zealand fellowships. Fieldwork was undertaken under ARC Linkage Project (LP120200724), supported by Linkage Partner Antarctic Logistics and Expeditions (ALE). JW and KW undertook GPR survey of the Patriot Hills record through NERC support with logistical field support from the British Antarctic Survey. SMD acknowledges financial support from Coleg Cymraeg Cenedlaethol and the European Research Council. KK was supported by JSPS KAKENHI. We thank Dr Chris Hayward and Dr Gwydion Jones for electron microprobe assistance, Kathryn Lacey and Gareth James for help with preparing the tephra samples, Drs Nelia Dunbar, Nels Iverson and Andrei Kurbatov for discussions on the tephra correlations, CSIRO GASLAB personnel for support of gas analysis, Prof. Bill Sturges and Dr Sam Allin of the Centre for Ocean and Atmospheric Sciences (University of East Anglia, UK) for performing the sulfur hexafluoride analyses, Levke Caesar (Potsdam Institute for Climate Impact Research) for preparing the recent trend in SSTs in Fig. 1, Vicki Taylor (British Ocean Sediment Core Research Facility, Southampton) for assistance with marine core sampling, and Dr Emilie Capron (British Antarctic Survey) for advice on reconstructing early southern Last Interglacial temperatures. CSIRO's contribution was supported in part by the Australian Climate Change Science Program (ACCSP), an Australian Government Initiative.

Author contributions

CSMT, CJF, NRG and RTJ conceived the research; CT, CJF, NRG, AC, LW, JY, SMD, PGA, CJM, RTJ, DE, MR, DPT, CBR, ZT, MB, NCM, MK, JW and KW designed the methods and performed the analysis; CT wrote the paper with input from all authors. There are no competing interests.

Fig. 1 Location and age profile of Patriot Hills blue ice area. (a) Location of Antarctic ice and marine records discussed in this study and austral spring-summer (October-March) sea surface temperature trends (over the period 1981-2010; HadISST data). (b) Trace gas (circles), tephra (triangles) and boundary (square) age solutions for surface ice along transect B-B' relative to an arbitrary datum along the transect (displayed in panel d). Dashed lines denote unconformities D0-D2 at their surface expression. (c) Basal topography of the Ellsworth Subglacial Highlands (West Antarctica) with the locations of airborne radio-echo sounding transect A-A' (displayed in panel e) and Rutford Ice Stream (IS)[18]. (d) The location of Patriot Hills in Horseshoe Valley (LIMA background image) with the BIA climate line (marked by transect B-B'), dominant ice flow direction and distance to grounding line. The Horseshoe Valley, Independence and Ellsworth troughs are given by the initials HV, IT and ET respectively. (e) Airborne radio-echo sounding cross section of ice within Horseshoe Valley, Independence and Ellsworth troughs (modified from ref. [18]. Digitization highlights basal topography (brown), lower basal ice unit (grey) and upper ice unit (red) as well as internal stratigraphic features (black for observed, dashed for inferred, and purple for best estimate).

Fig. 2 Climate, ocean circulation and sea level changes over the past 140 kyr. (a) $\delta^{18}O$ record from the North Greenland (NGRIP) ice core[8]. (b) Bermuda Rise $^{231}Pa/^{230}Th$ data (reversed axis; 1σ uncertainty) with dashed line denoting production ratio of 0.093 marking sluggish/absent AMOC[34]. Selected North Atlantic Heinrich (H) events and reduced AMOC shown. (c) Biogenic opal flux from ODP Site 1094 (53.2˚S) as a measure of wind-driven upwelling in the Southern Ocean[35]. (d) Comparison between the recently compiled global atmospheric methane time series (red line; 2σ envelope)[16] with the methane record from the West Antarctic Patriot Hills (black circles with 1σ uncertainty; open circles mark anomalously high concentration data excluded from age model). (e) Patriot Hills δD record with mean Holocene values; envelope 1σ. Grey shading denotes the timing of the surface elevation change across the Weddell Sea Embayment as indicated by the hiatus in the Patriot Hills sequence and inferred substantial Antarctic ice mass loss, consistent with the reported divergence of the isotopic signal observed between the horizontal Mount Moulton ice core record from the WAIS and East Antarctic ice cores [11,12,22], and peak global sea level[6]. Triangles denote the presence of geochemically-identified tephra layers in the Patriot Hills record. Pie-chart representation of percentage methane-utilising bacteria in 16S rRNA samples from Patriot Hills; crosses denote absence of these bacteria (Methods). (f) Temporal changes in ocean productivity with peak productivity (PP; green shading) during interglacials and subsequent enhanced content of calcareous microfossils in Antarctic continental margin sediments (red shading)[23]. Dashed black line shows position of tephra identified in the Patriot Hills (-340 m), Dome Fuji (1785.14 m) and Tephra B in marine sediments from the West Antarctic continental margin. (g) East Antarctic Dome Fuji $\delta^{18}O$ record[17,22]. (h) Reconstructed relative sea level curve with 2σ envelope[6]. Yellow shading highlights the timing of iceberg-rafted Heinrich debris event 11 (H11), when large amounts of iceberg-rafted debris were deposited in the North Atlantic[31] and the $^{231}Pa/^{230}Th$ ratio on Bermuda Rise shifted towards the production ratio of 0.093, representative of sluggish or absent AMOC[34]. Circled numbers 1 and 2 denote enhanced upwelling-induced warming in the Southern Ocean and Antarctic ice mass loss, respectively.

Fig. 3 Ocean-atmospheric interactions during Termination II and the Last Interglacial. Panels show changing Atlantic Meridional Overturning Circulation (AMOC) in response to iceberg discharge (a,b) in the North Atlantic (Heinrich event 11) during Termination II and (c) from the Antarctic Ice Sheets (AIS) during the Last Interglacial, with inferred shifts in atmospheric circulation including mid-latitude Southern Hemisphere westerly (crossed circle) airflow and Intertropical Convergence Zone (ITCZ)[10,31,35,38]. Vertical arrows denote CH_4 and heat flux associated with Antarctic coastal easterly (dot in circle) and westerly (crossed circle) airflow[19,36]. AABW, AAIW, NAIW and NADW define Antarctic Bottom Water, Antarctic Intermediate Water, North Atlantic Intermediate Water and North Atlantic Deep Water, respectively.

Fig. 4 Modelled Antarctic ice-sheet evolution under Last Interglacial forcing. (a) Sea-level equivalent mass loss for ice-sheet simulations forced by a range of air and ocean temperature anomalies relative to present day. 'dT' and 'dOT' describes atmospheric and ocean temperature anomalies respectively. (b-d) shows Antarctic Ice Sheet extent and elevation with 2˚C warmer ocean temperatures over time intervals of 1, 2 and 5 kyr, respectively (with no atmospheric warming); equivalent sea-level contribution is given in the bottom left corner of each panel. Locations of Patriot Hills (Ellsworth Mountains, West Antarctic Ice Sheet) and ice core records discussed in this study are shown in panel b. Inset box in (b) outlines region shown in Fig. 5.

Fig. 5 Bed (black line) and surface (blue) elevation changes at Patriot Hills (Ellsworth Mountains, West Antarctic Ice Sheet) in response to 2˚C warmer ocean temperatures over a time interval of 5 kyr (with no atmospheric warming) (a). Bed (black line) and surface (blue) elevation changes vs time, with phases of the prevalence of particular processes, such as ice-shelf collapse (mint shaded), regional uplift (grey shaded) and dynamic thinning (light-brown shaded), highlighted. (b-g) Selected time slices corresponding to dashed lines in panel a showing ice shelf extent and ice sheet elevation in the Weddell Sea Embayment (WSE) over the first 3 kyr. Location of Patriot Hills is marked by the red square; grey shaded areas are ice-shelf covered, whilst white areas are free of both grounded and floating glacial ice.

	1000 yrs	**2000 yrs**	**5000 yrs**	**10,000 yrs**
1˚C SST warming				
0˚C air	1.81	3.82	4.98	5.25
2˚C air	2.13	4.82	5.84	6.04
4˚C air	2.47	5.84	6.89	7.28
2˚C SST warming				
0˚C air	3.20	5.32	5.86	6.81
2˚C air	3.61	5.97	6.95	7.69
4˚C air	4.19	6.83	8.37	9.82
3˚C SST warming				
0˚C air	4.01	5.77	6.58	8.22
2˚C air	4.66	6.25	7.46	9.16
4˚C air	5.11	7.17	9.01	10.92

Table 1 Sea-level equivalent mass loss (metres) for Antarctic ice-sheet simulations forced over 10,000 years by range of annual air and ocean temperature anomalies relative to present day.

METHODS

Patriot Hills

Site description and geomorphological context. The Patriot Hills BIA (Horseshoe Valley, Ellsworth Mountains; 80°18′S, 81°21′W) is a slow flowing (<12 m yr^{-1}) compound glacier system situated within an over-deepened catchment that coalesces with the Institute Ice Stream at the periphery of the WSE[18,26,48-50] (Figs 1, S1-S3) (SI). Airborne radio-echo sounding (RES) surveys across the Ellsworth Mountains have revealed several wide (up to 34 km across) and long (260 km) subglacial troughs containing ice up to 2620 m thick (Fig. 1)[18], along the side of which, two radar zones have been interpreted to indicate layers of ice with contrasting physical properties, consistent with snow deposited during previous glacial/interglacial transitions. In the lee of a small mountain chain at the end of Horseshoe Valley called Patriot Hills, strong local katabatic winds descend into the valley from the polar plateau, ablating the ice sheet surface by up to 170 kg m^{-2} yr^{-1} (ref. [50]). As a result, ancient ice is drawn up from depth in the Horseshoe Valley Trough to form an extensive BIA (more than 1150m across; Supplementary Fig. 3)[26,27,51]. High-resolution analysis using ground-penetrating radar (GPR)[26] and isotopes identifies three distinct unconformities (surface distances relative to an arbitrary transect datum): 247 m (D1), 360 m (D2), and -339 m (D0). Based on the trace gas, tephra and isotopic values of the surface ice beyond D0 (closest to Patriot Hills) we interpret this section of the record to be Termination II in age (see below).

Previous work has interpreted erosional features D1 and D2 in the Patriot Hills BIA to be a consequence of extensive ice surface lowering in Horseshoe Valley (up to ~500 m since the Last Glacial Maximum, 21 kyr) and more exposure of katabatic-enhancing nunataks, resulting in increased wind scour[20,26]. Whilst this scenario may explain unconformity D0, other studies have demonstrated Horseshoe Valley and the wider WSE to be highly sensitive to periods of rapid ice stream advance or retreat in the last glacial cycle and Holocene with dramatic reductions in surface elevation[20,26-28]. Recent work investigating the impact of ice shelf loss on glaciers along the Antarctic Peninsula provides important insights, albeit on a smaller scale. The 2002 Larsen B ice shelf collapse led to many of the tributary glaciers abruptly changing from a convex to a concave profile[29], with relic ice left isolated on the upper flanks of the valleys[30]. Under a scenario of extreme ice surface lowering arising from ocean warming during the early Last Interglacial, the ice at Patriot Hills preserves a record of glacier flow in Horseshoe Valley up to the moment when the Filcher-Ronne Ice Shelf collapsed, after which the sequence likely remained isolated for multiple millennia until the ice surface had risen sufficiently to reincorporate the isolated ice into the glacier sometime during late MIS 5. Our ancient DNA (notably the detection of *Methyloversatilis* microbes in the sample form -340 m in the Patriot Hills record) and ice sheet modelling are consistent with early offshore warming and substantial ice mass loss in the early Last Interglacial[23,32,33], preserving most (if not all) of the Termination II ice record during the period represented by the D0 unconformity (see below). We therefore consider D0 reflects a significant fall in surface elevation and change in flow direction due to isostatically-driven isolation of the valley during a period of rapid draw down of the ice streams across the WSE.

Chronology. Chronological control across the transect is provided by a comprehensive suite of trace gas samples – carbon dioxide (CO_2), methane (CH_4) and nitrous oxides (N_2O) – and volcanic tephra horizons. The trace gas measurements provide a range of possible age solutions against the recently published 156-kyr smoothed global time series for these gas species[16], which together with the absolute constraints provided by the tephra horizons, allows the development of a robust chronological framework that can be tied directly to the isotopic series through high-resolution GPR[26,51] (Supplementary Fig. 4). A Kovacs 9 cm diameter ice corer was used to collect ice for gas and taken from >3 m depth to minimise modern air contamination and/or alteration[51]. The samples were double bagged and sealed in the field, and transported frozen to CSIRO's ICELAB facility in Melbourne for the extraction and measurement of trace gases using a modified dry extraction 'cheese grater' and cryogenic trapping technique[52,53]. The trapped air samples were analysed by gas chromatography (GC) and the trace gas concentrations are reported against the calibration scales maintained by CSIRO GASLAB[54]. Where sufficient material was available, duplicates were analysed.

The presence of visible tephra layers (volcanic ash horizons) provides additional chronological control for the Patriot Hills BIA. Here we report two new tephras from Patriot Hills at 10 m and -340 m, both observed as ~4 cm units of dispersed shards (Supplementary Fig. 7). Shards were extracted by centrifugation of the melted ice samples and put onto a glass slide for electron microprobe analysis. The slides were ground and polished using silica carbide paper and decreasing grades of diamond suspension to expose fresh sections of glass. Single-grain analyses of ten oxides were performed on a Cameca SX-100 electron microprobe at the Tephrochronology Analytical Unit, University of Edinburgh. See SI for operating conditions[55]. Geochemical results are provided in Supplementary Table 1. The shards from 10 m are bimodal, with a basanitic and trachytic composition (Supplementary Fig. 8). The shards from -340 m are trachytic in composition and exhibit a tightly-clustered population (Supplementary Fig. 9). Both were compared to published tephras from across Antarctica[23,56-66]. The 10 m tephra has the closest match to be the basanite Tephra C from the WAIS Divide at 3149.12 m (Similarity Coefficient or SC = 0.98), equivalent to 44.9±0.3 kyr[66]. The -340 m tephra revealed the closest match to a tephra layer in the Dome Fuji ice core at 1785.14 m depth (SC = 0.966; equivalent to 130.7±1.8 kyr on the AICC2012 timescale[17,59,67]; data previously unpublished).

A widespread tephra found in marine sedimentary records on the West Antarctic continental margin (Tephra B) has been proposed to correlate to the tephra at Dome Fuji 1785.14 m but the correlation has until now remained only tentative in the absence of any reported geochemistry from the latter[23]. Here we find the major oxides from Tephra B have a close match to Patriot Hills -340 m (SC = 0.948), consistent with this interpretation. To test this correlation, we undertook trace element analysis of the glass shards from Patriot Hills at -340 m. Unfortunately, the Dome Fuji shards were too thin for analysis. However, we were able to undertake trace element analyses on Tephra B samples from two marine sediment cores from the West Antarctic continental margin: PC108 (4.65 m depth) and PC111 (6.86 m depth)[23]. Trace element analysis of volcanic glass shards were performed using an Agilent 8900 triple quadrupole ICP-MS (ICP-QQQ) coupled to a Resonetics 193nm ArF excimer laser-ablation in the Department of Earth Sciences, Royal Holloway, University of London. See SI for operating conditions[68]. Accuracies of LA-ICP-MS analyses of ATHO-G and reference StHs6/80-G MPI-DING[69] glass were typically ≤ 5%. Identical trace element glass chemistries (Supplementary Fig. 11, Supplementary Table 2) strongly support the correlation of Patriot Hills -340 m tephra horizon and the marine West Antarctic Tephra B (ref. [23]) which is in turn correlated to Dome Fuji 1785.14 m (ref. [22,23,59,67]), and probably originates from the

Marie Byrd Land volcanic province (West Antarctica)[23]. The recognition of a widespread tephra horizon across a large sector of the Antarctic at the very onset of the LIG provides a time-parallel marker horizon crucial for future studies investigating Antarctic ice-sheet mass loss.

To develop an age model we undertook Bayesian age modelling using a Poisson process deposition model (P_sequence) in the software package OxCal v.4.2.4 (https://c14.arch.ox.ac.uk/) (Supplementary Tables 3 and 4)[70,71]. Using Bayes theorem, the algorithms employed sample possible solutions with a probability that is the product of the prior and likelihood probabilities[72,73]. 'Calibration curves' with 20 year resolution were developed for the three trace gas species using the 156 kyr time series[16]. Taking into account the deposition model, the reported ages of the tephra layers, and the common age solutions offered by the trace gas measurements, the posterior probability densities quantify the most probable age distributions. The available constraints suggest the 1156-m long Patriot Hills BIA transect spans time intervals from ~134.2 to ~1.3 kyr comprising four key zones: 4 (-362 to -339 m, equivalent to 134.2±2.2 to 130.1±1.8 kyr), 3 (-326 to 240 m, equivalent to 80±6.1 to 22.7±2.8 kyr), 2 (240 to 360 m, equivalent to 22.7±2.8 to 10.3±0.4 kyr) and 1 (360 to 800 m, 10.3±0.4 to 1.3±0.6 kyr). The Agreement Index for the Patriot Hills age model was 101.6% ($A_{overall}$=71.2%), exceeding the recommended rejection Agreement Index threshold of 60% (ref. [71]) (Methods).

Isotopes. δD and $\delta^{18}O$ isotopic measurements were performed between 1 and 3 m resolution at James Cook University (JCU) using Diffusion Sampling - Cavity Ring-down Spectrometry (DS-CRDS) (International Atomic Energy WICO Lab ID. 16139)[74]. This system continuously converts liquid water into water vapour for realtime stable isotope analysis by laser spectroscopy (Picarro L2120-i, Sunnyvale, CA, USA). See SI for operating conditions. To ensure reproducibility, a subset of samples was rerun at UNSW ICELAB for δD and $\delta^{18}O$ using a Los Gatos Research Liquid Water Isotope Analyser 24d (International Atomic Energy WICO Lab ID. 16117). Reported overall analytical precision on long term ice core standards is <0.32‰ for δD and <0.13 for $\delta^{18}O$ values. All isotopic values are expressed relative to the Vienna Standard Mean Ocean Water 2 (VSMOW2).

Ancient DNA analysis. BIAs offer the novel opportunity to process large volume samples of continental Antarctic ice in the field (~7 kg per temporal sample), creating a new prospect of generating sufficient microbial concentrations to permit detailed genetic biodiversity surveys[39,40] (Fig. 2). To obtain the samples, a Kovac corer was thoroughly cleaned with 1-3% bleach and wiped with 95% ethanol between core extractions to minimise cross contamination. After coring, the top 1 m of ice was removed and discarded, before 1-2 m long cores were collected in 50 cm sections and immediately placed into clean PFTE flexible plastic tubing. A heat sealer was used to close the tubing at the top and bottom of the core. The sealed core was then cut from the remaining tubing with a sterile blade, and the process was repeated to encase the core in a second layer of the plastic tubing for protection during transport. Within 1-6 hours of extraction the tubing-encased BIA cores were hung inside a large dome tent to melt via solar radiation over 12-24 hours, using black plastic bin liners around the plastic tubing to speed up the process where necessary. The melted BIA sample was transferred from the inside layer of tubing directly into a hand-powered vacuum filtration system cleaned with 1-3% bleach and ethanol wipes between samples. For each sample, disposable, sterile, 0.45 μm nitrocellulose filters were used to filter and collect whole bacterial organisms trapped in the ice during its formation, and reduce noise caused by environmental DNA. Filters were stored in sterile plastic bags, frozen at -20°C, and returned to the Australian Centre for Ancient DNA (ACAD) in Adelaide for ultra-clean genetic analysis.

Strict ancient DNA methodologies designed to assess low-biomass microbial samples were applied[75] (see SI for detailed methodology and analysis). DNA from all ice samples as well as extensive sampling and laboratory controls were extracted using two methods to maximise species recovery, and 16S ribosomal RNA libraries were amplified in triplicate using published, universal bacterial and archaeal 16S ribosomal RNA (rRNA) primers. After DNA sequencing, all individually indexed 16S rRNA libraries were de-multiplexed, quality filtered, and imported into QIIME v.1.8.0. Microbial taxa were identified by comparing sequences to the Geengenes v13 reference database and binning sequences with 97% similar to known species into Operational Taxonomic Units (OTUs) using closed reference clustering in UCLUST. Sampling and laboratory contaminants were then filtered from ice samples, and an average of 30.8% of the reads for each sample were retained (Supplementary Table 5). Retained sequences were then pooled, and the resulting taxa present in each sample were explored as a proportion of the total filtered DNA sequencing reads. Alpha and beta diversity was explored in QIIME, and importantly, no statistically significant differences in diversity were detected across the samples. While the current sample numbers limit resolution, our study highlights the untapped potential of BIA genetic data to exploit cryosphere microbial communities to investigate glaciological and environmental change[40].

Ice-sheet modelling

To investigate former ice sheet dynamics around the Patriot Hills and across Antarctica we take a range of values for polar ocean warming (1˚-3˚C)[7,9,15] and employed the Parallel Ice Sheet Model (PISM) v.0.6.3 (ref. [2]), an open source three-dimensional, thermomechanical coupled ice-sheet/ice-shelf model. PISM employs a stress balance that superposes solutions of the shallow-ice and shallow-shelf equations, and incorporates a pseudo-plastic basal substrate rheology to allow for realistic sliding over meltwater saturated sediments, a three-dimensional bed deformation model to account for changes in ice loading through time, and a sub-grid basal traction and driving stress interpolation scheme to allow realistic grounding-line motion[76,77]. In the experiments presented here we chose not to implement the sub-grid scale interpolated ice shelf basal melt component of this scheme[2,78]. Calving is parameterised using horizontal strain rates and a minimum thickness criterion[79,80]. Our experimental methodology is identical to that described in detail elsewhere[81,82]. Climate and ocean temperature perturbations are applied as spatially-uniform linear increments added to boundary distributions representing present-day conditions. Linear increases take place between 2000 and 3000 model years. The first 2000 years (no forcing) allow any transient behaviour associated with model initialisation to take place in the absence of environmental perturbations, whereas the subsequent 1000 years force the ice sheet to evolve slowly to changes in air and ocean temperature and precipitation. All experiments are run at a spatial resolution of 20 km.

Reconstructed summer sea surface temperature anomalies relative to present day (the 1998 World Ocean Atlas)[9] were used to mimic a range of warmer LIG conditions and applied to a stable modern configuration of the Antarctic Ice Sheet (Table 1). A limitation of this approach is that the transient history from the preceding glacial state is not simulated. However, for the response of the ice shelves this colder prehistory should not be critical, and the experiments as performed are directly relevant for the future of the ice sheets. From these simulations we extract data from the first 10 kyr. The ice-sheet modelling outputs support the view that ocean warming was the primary driver of substantial early LIG mass loss in Patriot Hills and across large parts of Antarctica, a view reinforced by the e-folding time on the 2˚C ocean warming scenario (with no atmospheric warming) of 1400 years, which yields c. 4.5 m GMSL.

References

1 Ritz, C. *et al*. Potential sea-level rise from Antarctic ice-sheet instability constrained by observations. *Nature* **528**, 115-118 (2015).

2 Golledge, N. R. *et al*. The multi-millennial Antarctic commitment to future sea-level rise. *Nature* **526**, 421-425 (2015).

3 DeConto, R. M. & Pollard, D. Contribution of Antarctica to past and future sea-level rise. *Nature* **531**, 591-597 (2016).

4 Dutton, A. *et al*. Sea-level rise due to polar ice-sheet mass loss during past warm periods. *Science* **349**, 153 (2015).

5 Mercer, J. H. West Antarctic ice sheet and CO_2 greenhouse effect: a threat of disaster. *Nature* **271**, 321-325 (1978).

6 Grant, K. M. *et al*. Sea-level variability over five glacial cycles. *Nature Communications* **5**, 5076 (2014).

7 Turney, C. S. M. & Jones, R. T. Does the Agulhas Current amplify global temperatures during super-interglacials? *Journal of Quaternary Science* **25**, 839-843 (2010).

8 NEEM Community Members. Eemian interglacial reconstructed from a Greenland folded ice core. *Nature* **493**, 489-494 (2013).

9 Capron, E., Govin, A., Feng, R., Otto-Bliesner, B. L. & Wolff, E. W. Critical evaluation of climate syntheses to benchmark CMIP6/PMIP4 127 ka Last Interglacial simulations in the high-latitude regions. *Quaternary Science Reviews* **168**, 137-150 (2017).

10 Fogwill, C. J. *et al*. Testing the sensitivity of the East Antarctic Ice Sheet to Southern Ocean dynamics: past changes and future implications. *Journal of Quaternary Science* **29**, 91-98 (2014).

11 Korotkikh, E. V. *et al*. The last interglacial as represented in the glaciochemical record from Mount Moulton Blue Ice Area, West Antarctica. *Quaternary Science Reviews* **30**, 1940-1947 (2011).

12 Steig, E. J. *et al*. Influence of West Antarctic Ice Sheet collapse on Antarctic surface climate. *Geophysical Research Letters* **42**, 4862-4868 (2015).

13 Kingslake, J. *et al*. Extensive retreat and re-advance of the West Antarctic Ice Sheet during the Holocene. *Nature* **558**, 430-434 (2018).

14 Sutter, J., Gierz, P., Grosfeld, K., Thoma, M. & Lohmann, G. Ocean temperature thresholds for Last Interglacial West Antarctic Ice Sheet collapse. *Geophysical Research Letters* **43**, 2675–2682 (2016).

15 Hoffman, J. S., Clark, P. U., Parnell, A. C. & He, F. Regional and global sea-surface temperatures during the last interglaciation. *Science* **355**, 276-279 (2017).

16 Köhler, P., Nehrbass-Ahles, C., Schmitt, J., Stocker, T. F. & Fischer, H. A 156 kyr smoothed history of the atmospheric greenhouse gases CO_2, CH_4, and N_2O and their radiative forcing. *Earth Syst. Sci. Data* **9**, 363-387 (2017).

17 Veres, D. *et al*. The Antarctic ice core chronology (AICC2012): an optimized multi-parameter and multi-site dating approach for the last 120 thousand years. *Climate of the Past* **9**, 1733-1748 (2013).

18 Winter, K. *et al*. Airborne radar evidence for tributary flow switching in Institute Ice Stream, West Antarctica: implications for ice sheet configuration and dynamics. *Journal of Geophysical Research: Earth Surface* **120**, 1611-1625 (2015).

19 Wadham, J. L. *et al*. Potential methane reservoirs beneath Antarctica. *Nature* **488**, 633-637 (2012).

20 Fogwill, C. J. *et al*. Drivers of abrupt Holocene shifts in West Antarctic ice stream direction determined from combined ice sheet modelling and geologic signatures. *Antarctic Science* **26**, 674-686 (2014).

21 Bradley, S. L., Siddall, M., Milne, G. A., Masson-Delmotte, V. & Wolff, E. Where might we find evidence of a Last Interglacial West Antarctic Ice Sheet collapse in Antarctic ice core records? *Global and Planetary Change* **88-89**, 64-75 (2012).

22 Uemura, R. *et al*. Asynchrony between Antarctic temperature and CO_2 associated with obliquity over the past 720,000 years. *Nature Communications* **9**, 961 (2018).

23 Hillenbrand, C.-D. *et al*. Volcanic time-markers for Marine Isotopic Stages 6 and 5 in Southern Ocean sediments and Antarctic ice cores: implications for tephra correlations between palaeoclimatic records. *Quaternary Science Reviews* **27**, 518-540 (2008).

24 Ross, N. *et al*. Steep reverse bed slope at the grounding line of the Weddell Sea sector in West Antarctica. *Nature Geosci* **5**, 393-396 (2012).

25 Hein, A. S. *et al*. Evidence for the stability of the West Antarctic Ice Sheet divide for 1.4 million years. *Nature Communications* **7**, 10325 (2016).

26 Winter, K. *et al*. Assessing the continuity of the blue ice climate record at Patriot Hills, Horseshoe Valley, West Antarctica. *Geophysical Research Letters* **43**, 2019-2026 (2016).

27 Fogwill, C. J. *et al*. Antarctic ice sheet discharge driven by atmosphere-ocean feedbacks at the Last Glacial Termination. *Scientific Reports* **7**, 39979, doi: 39910.31038/srep39979 (2017).

28 Siegert, M., Ross, N., Corr, H., Kingslake, J. & Hindmarsh, R. Late Holocene ice-flow reconfiguration in the Weddell Sea sector of West Antarctica. *Quaternary Science Reviews* **78**, 98-107 (2013).

29 Shuman, C. A., Berthier, E. & Scambos, T. A. 2001–2009 elevation and mass losses in the Larsen A and B embayments, Antarctic Peninsula. *Journal of Glaciology* **57**, 737-754 (2011).

30 Rott, H. *et al*. Changing pattern of ice flow and mass balance for glaciers discharging into the Larsen A and B embayments, Antarctic Peninsula, 2011 to 2016. *The Cryosphere* **12**, 1273-1291 (2018).

31 Marino, G. *et al*. Bipolar seesaw control on last interglacial sea level. *Nature* **522**, 197-201 (2015).

32 Dutton, A., Webster, J. M., Zwartz, D., Lambeck, K. & Wohlfarth, B. Tropical tales of polar ice: evidence of Last Interglacial polar ice sheet retreat recorded by fossil reefs of the granitic Seychelles islands. *Quaternary Science Reviews* **107**, 182-196 (2015).

33 Hayes, C. T. *et al*. A stagnation event in the deep South Atlantic during the last interglacial period. *Science* **346**, 1514-1517 (2014).

34 Böhm, E. *et al*. Strong and deep Atlantic meridional overturning circulation during the last glacial cycle. *Nature* **517**, 73-76 (2015).

35 Jaccard, S. L. *et al*. Two modes of change in Southern Ocean productivity over the past million years. *Science* **339**, 1419-1423 (2013).

36 Rintoul, S. R. The global influence of localized dynamics in the Southern Ocean. *Nature* **558**, 209-218 (2018).

37 Hellmer, H. H., Kauker, F., Timmermann, R., Determann, J. & Rae, J. Twenty-first-century warming of a large Antarctic ice-shelf cavity by a redirected coastal current. *Nature* **485**, 225-228 (2012).

38 Jones, R. T. *et al*. Delayed maximum northern European summer temperatures during the Last Interglacial as a result of Greenland Ice Sheet melt. *Geology* **45**, 23-26 (2017).

39 Santibáñez, P. A. *et al*. Prokaryotes in the WAIS Divide ice core reflect source and transport changes between Last Glacial Maximum and the early Holocene. *Global Change Biology* **24**, 2182-2197 (2018).

40 Boetius, A., Anesio, A. M., Deming, J. W., Mikucki, J. A. & Rapp, J. Z. Microbial ecology of the cryosphere: sea ice and glacial habitats. *Nature Reviews Microbiology* **13**, 677 (2015).

41 Kalyuzhnaya, M. G. *et al*. *Methyloversatilis universalis* gen. nov., sp. nov., a novel taxon within the Betaproteobacteria represented by three methylotrophic isolates. *International Journal of Systematic and Evolutionary Microbiology* **56**, 2517-2522 (2006).

42 Kawamura, K. *et al*. Northern Hemisphere forcing of climatic cycles in Antarctica over the past 360,000 years. *Nature* **448**, 912–916 (2007).

43 Schneider, R., Schmitt, J., Köhler, P., Joos, F. & Fischer, H. A reconstruction of atmospheric carbon dioxide and its stable carbon isotopic composition from the penultimate glacial maximum to the last glacial inception. *Climate of the Past* **9**, 2507-2523 (2013).

44 Eggleston, S., Schmitt, J., Bereiter, B., Schneider, R. & Fischer, H. Evolution of the stable carbon isotope composition of atmospheric CO_2 over the last glacial cycle. *Paleoceanography* **31**, 434-452 (2016).

45 Mengel, M., Feldmann, J. & Levermann, A. Linear sea-level response to abrupt ocean warming of major West Antarctic ice basin. *Nature Climate Change* **6**, 71-74 (2015).

46 Shepherd, A., Fricker, H. A. & Farrell, S. L. Trends and connections across the Antarctic cryosphere. *Nature* **558**, 223-232 (2018).

47 Caesar, L., Rahmstorf, S., Robinson, A., Feulner, G. & Saba, V. Observed fingerprint of a weakening Atlantic Ocean overturning circulation. *Nature* **556**, 191-196 (2018).

48 Bingham, R. G. *et al*. Ice-flow structure and ice dynamic changes in the Weddell Sea sector of West Antarctica from radar-imaged internal layering. *Journal of Geophysical Research: Earth Surface* **120**, 655-670 (2015).

49 Rignot, E., Mouginot, J. & Scheuchl, B. (ed NASA National Snow and Ice Data Center Distributed Active Archive Center) (Boulder, Colorado, USA, 2017).

50 Casassa, G. *et al*. Elevation change and ice flow at Horseshoe Valley, Patriot Hills, West Antarctica. *Annals of Glaciology* **39**, 20-28 (2004).

51 Turney, C. *et al*. Late Pleistocene and early Holocene change in the Weddell Sea: a new climate record from the Patriot Hills, Ellsworth Mountains, West Antarctica. *Journal of Quaternary Science* **28**, 697-704 (2013).

52 Etheridge, D. M. *et al*. Natural and anthropogenic changes in atmospheric CO_2 over the last 1000 years from air in Antarctic ice and firn. *Journal of Geophysical Research: Atmospheres* **101**, 4115-4128 (1996).

53 Rubino, M. *et al*. A revised 1000 year atmospheric $\delta^{13}C$-CO_2 record from Law Dome and South Pole, Antarctica. *Journal of Geophysical Research* **118**, 1-18 (2013).

54 Francey, R. *et al*. in *Baseline Atmospheric Program Australia 1999-2000* (eds NW Tindale, N Derek, & PJ Fraser) 42-53 (Bureau of Meteorology and CSIRO Atmospheric Research, 2003).

55 Hayward, C. High spatial resolution electron probe microanalysis of tephras and melt inclusions without beam-induced chemical modification. *The Holocene* **22**, 119-125 (2012).

56 Narcisi, B., Petit, J. R., Delmonte, B., Basile-Doelsch, I. & Maggi, V. Characteristics and sources of tephra layers in the EPICA-Dome C ice record (East Antarctica): Implications for past atmospheric circulation and ice core stratigraphic correlations. *Earth and Planetary Science Letters* **239**, 253-265 (2005).

57 Narcisi, B., Petit, J. R. & Delmonte, B. Extended East Antarctic ice-core tephrostratigraphy. *Quaternary Science Reviews* **29**, 21-27 (2010).

58 Narcisi, B., Petit, J. R. & Tiepolo, M. A volcanic marker (92 ka) for dating deep east Antarctic ice cores. *Quaternary Science Reviews* **25**, 2682-2687 (2006).

59 Kohno, M., Fujii, Y. & Hirata, T. Chemical composition of volcanic glasses in visible tephra layers found in a 2503 m deep ice core from Dome Fuji, Antarctica. *Annals of Glaciology* **39**, 576-584 (2004).

60 Dunbar, N. W., McIntosh, W. C. & Esser, R. P. Physical setting and tephrochronology of the summit caldera ice record at Mount Moulton, West Antarctica. *Geological Society of America Bulletin* **120**, 796-812 (2008).

61 Dunbar, N. W. & Kurbatov, A. V. Tephrochronology of the Siple Dome ice core, West Antarctica: correlations and sources. *Quaternary Science Reviews* **30**, 1602-1614 (2011).

62 Narcisi, B., Petit, J. R., Langone, A. & Stenni, B. A new Eemian record of Antarctic tephra layers retrieved from the Talos Dome ice core (Northern Victoria Land). *Global and Planetary Change* **137**, 69-78 (2016).

63 Narcisi, B., Petit, J. R., Delmonte, B., Scarchilli, C. & Stenni, B. A 16,000-yr tephra framework for the Antarctic ice sheet: a contribution from the new Talos Dome core. *Quaternary Science Reviews* **49**, 52-63 (2012).

64 Narcisi, B., Petit, J. R. & Chappellaz, J. A 70 ka record of explosive eruptions from the TALDICE ice core (Talos Dome, East Antarctic plateau). *Journal of Quaternary Science* **25**, 844-849 (2010).

65 Basile, I., Petit, J. R., Touron, S., Grousset, F. E. & Barkov, N. Volcanic layers in Antarctic (Vostok) ice cores: Source identification and atmospheric implications. *Journal of Geophysical Research-Atmospheres* **106**, 31915-31931 (2001).

66 Iverson, N. A. *et al*. The first physical evidence of subglacial volcanism under the West Antarctic Ice Sheet. *Scientific Reports* **7**, 11457 (2017).

67 Fujita, S., Parrenin, F., Severi, M., Motoyama, H. & Wolff, E. Volcanic synchronization of Dome Fuji and Dome C Antarctic deep ice cores over the past 216 kyr. *Climate of the Past* **11**, 1395-1416 (2015).

68 Tomlinson, E., Thordarson, T., Müller, W., Thirlwall, M. & Menzies, M. Microanalysis of tephra by LA-ICP-MS—strategies, advantages and limitations assessed using the Thorsmörk Ignimbrite (Southern Iceland). *Chemical Geology* **279**, 73-89 (2010).

69 Jochum, K. P. *et al*. MPI-DING reference glasses for *in situ* microanalysis: New reference values for element concentrations and isotope ratios. *Geochemistry, Geophysics, Geosystems* **7** (2006).

70 Bronk Ramsey, C. & Lee, S. Recent and planned developments of the program OxCal. *Radiocarbon* **55**, 720-730 (2013).

71 Bronk Ramsey, C. Dealing with outliers and offsets in radiocarbon dating. *Radiocarbon* **51**, 1023-1045 (2009).

72 Higham, T. *et al*. The timing and spatiotemporal patterning of Neanderthal disappearance. *Nature* **512**, 306-309 (2014).

73 Bronk Ramsey, C. Probability and dating. *Radiocarbon* **40**, 461-474 (1998).

74 Munksgaard, N. C., Wurster, C. M. & Bird, M. I. Continuous analysis of $\delta^{18}O$ and δD values of water by diffusion sampling cavity ring-down spectrometry: A novel sampling device for unattended field monitoring of precipitation, ground and surface waters. *Rapid Communications in Mass Spectrometry* **25**, 3706-3712 (2011).

75 Adler, C. J. *et al*. Sequencing ancient calcified dental plaque shows changes in oral microbiota with dietary shifts of the Neolithic and Industrial revolutions. *Nature Genetics* **45**, 450 (2013).

76 Feldmann, J., Albrecht, T., Khroulev, C., Pattyn, F. & Levermann, A. Resolution-dependent performance of grounding line motion in a shallow model compared with a full-Stokes model according to the MISMIP3d intercomparison. *Journal of Glaciology* **60**, 353-360 (2014).

77 Bueler, E. & Brown, J. Shallow shelf approximation as a "sliding law" in a thermomechanically coupled ice sheet model. *Journal of Geophysical Research: Earth Surface* **114**, doi: 10.1029/2008JF001179 (2009).

78 Martin, M. A., Levermann, A. & Winkelmann, R. Comparing ice discharge through West Antarctic Gateways: Weddell vs. Amundsen Sea warming. *The Cryosphere Discuss*. **2015**, 1705-1733 (2015).

79 Albrecht, T. & Levermann, A. Fracture field for large-scale ice dynamics. *Journal of Glaciology* **58**, 165-176 (2012).

80 Levermann, A. *et al*. Kinematic first-order calving law implies potential for abrupt ice-shelf retreat. *The Cryosphere* **6**, 273-286 (2012).

81 Aitken, A. R. A. *et al*. Repeated large-scale retreat and advance of Totten Glacier indicated by inland bed erosion. *Nature* **533**, 385-389 (2016).

82 Golledge, N. R., Levy, R. H., McKay, R. M. & Naish, T. R. East Antarctic ice sheet most vulnerable to Weddell Sea warming. *Geophysical Research Letters* **44**, 2343-2351 (2017).

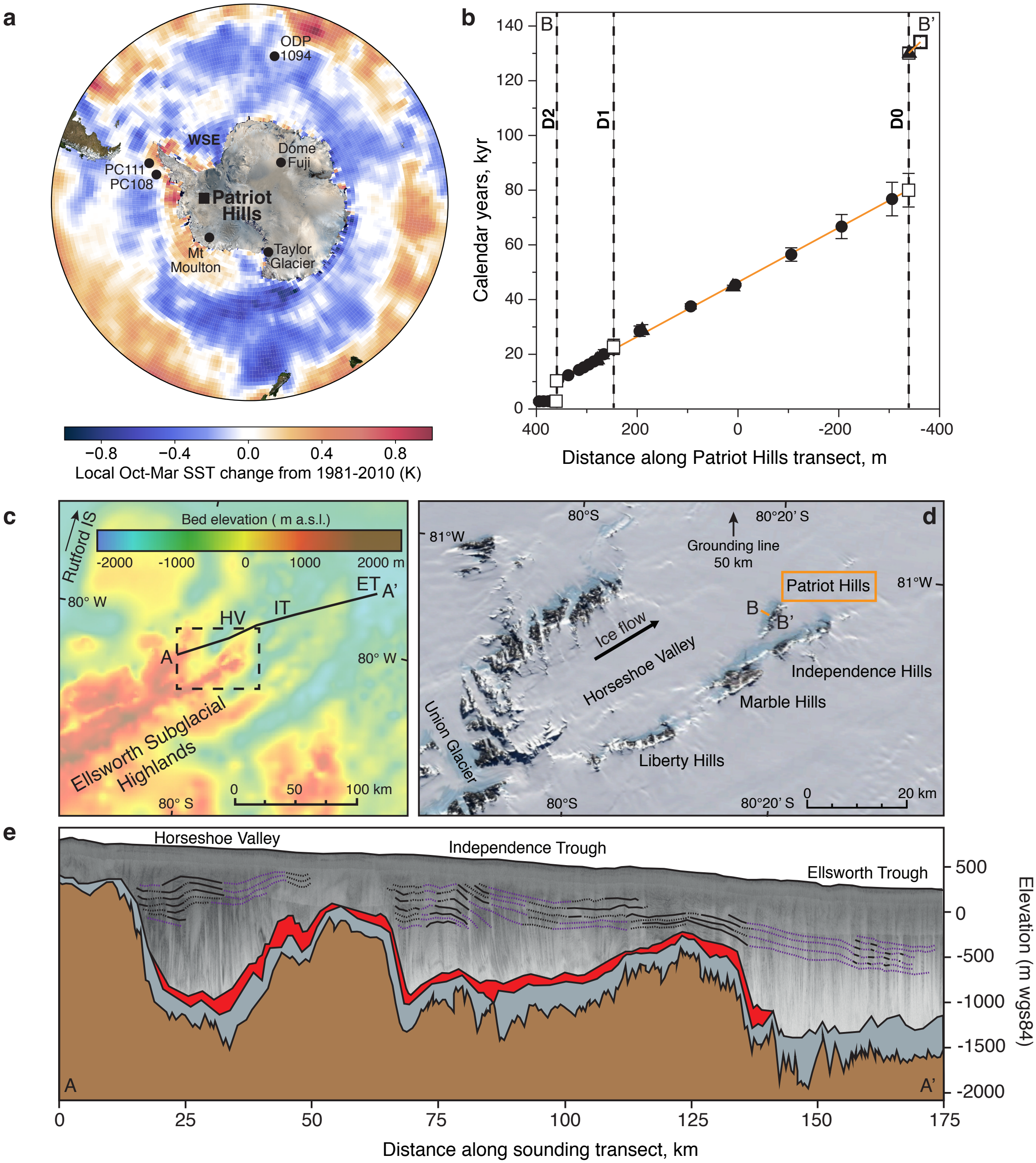

a
ODP 1094
WSE
Dome Fuji
PC111
PC108
Patriot Hills
Mt Moulton
Taylor Glacier
−0.8
−0.4
0.0
0.4
0.8
Local Oct-Mar SST change from 1981-2010 (K)
b
B
B'
D2
D1
D0
Calendar years, kyr
Distance along Patriot Hills transect, m
c
Rutford IS
Bed elevation (m a.s.l.)
-2000
-1000
0
1000
2000 m
80° W
ET
A'
HV
IT
A
Ellsworth Subglacial Highlands
80° S
0
50
100 km
d
80°S
80°20' S
81°W
Grounding line 50 km
Patriot Hills
Ice flow
Horseshoe Valley
Independence Hills
Marble Hills
Union Glacier
Liberty Hills
20 km
e
Horseshoe Valley
Independence Trough
Ellsworth Trough
Elevation (m wgs84)
Distance along sounding transect, km

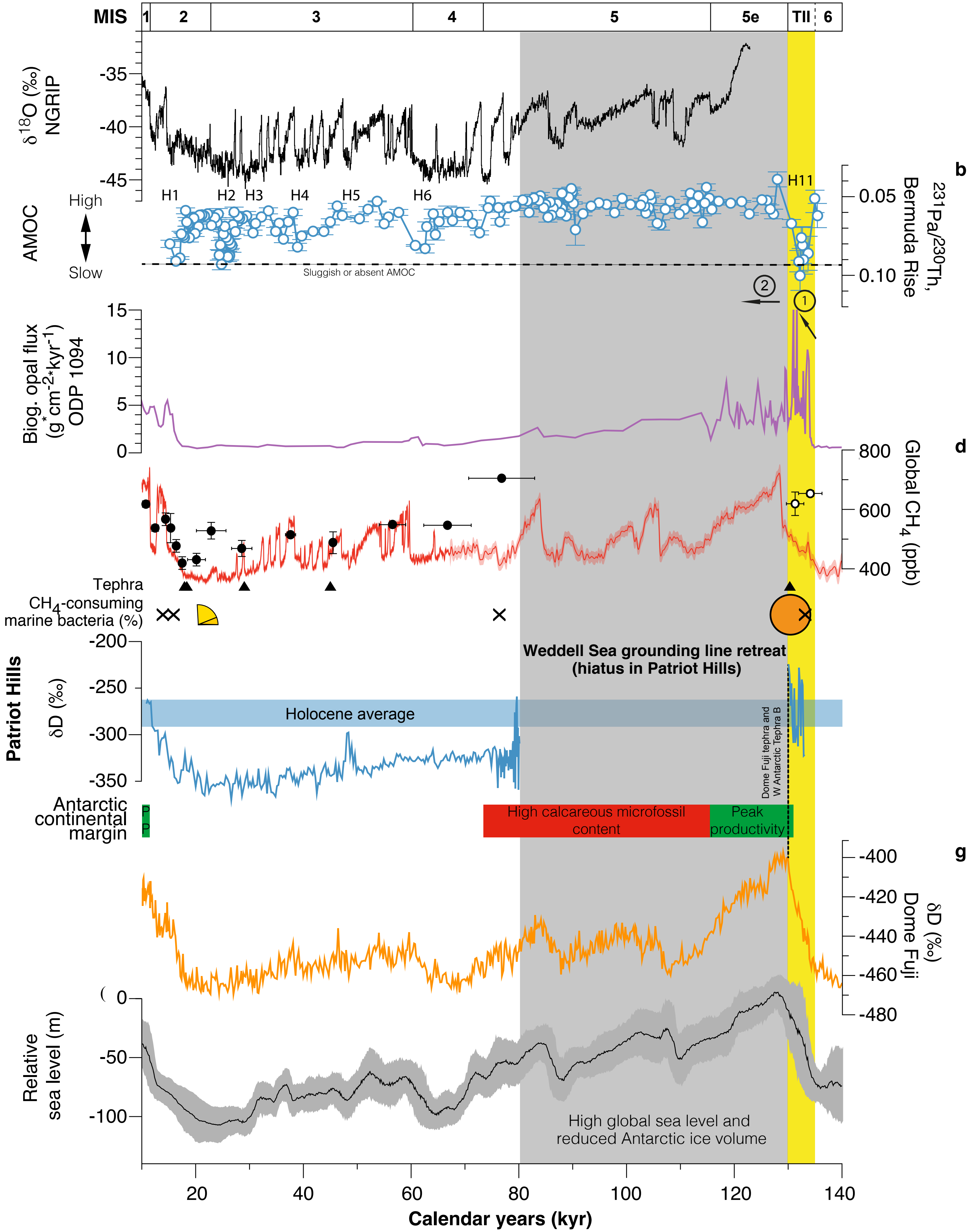

MIS
1
2
3
4
5
5e
TII
6
a
δ18O (‰) NGRIP
-35
-40
-45
b
231Pa/230Th, Bermuda Rise
0.05
0.10
AMOC
High
Slow
H1
H2
H3
H4
H5
H6
H11
Sluggish or absent AMOC
2
1
c
Biog. opal flux (g*cm-2*kyr-1) ODP 1094
15
10
5
0
d
Global CH4 (ppb)
800
600
400
e
Tephra
CH4-consuming marine bacteria (%)
Weddell Sea grounding line retreat (hiatus in Patriot Hills)
Patriot Hills
δD (‰)
-200
-250
-300
-350
Holocene average
Dome Fuji tephra and W Antarctic Tephra B
f
Antarctic continental margin
P
P
High calcareous microfossil content
Peak productivity
g
δD (‰) Dome Fuji
-400
-420
-440
-460
-480
h
Relative sea level (m)
0
-50
-100
High global sea level and reduced Antarctic ice volume
20
40
60
80
100
120
140
Calendar years (kyr)

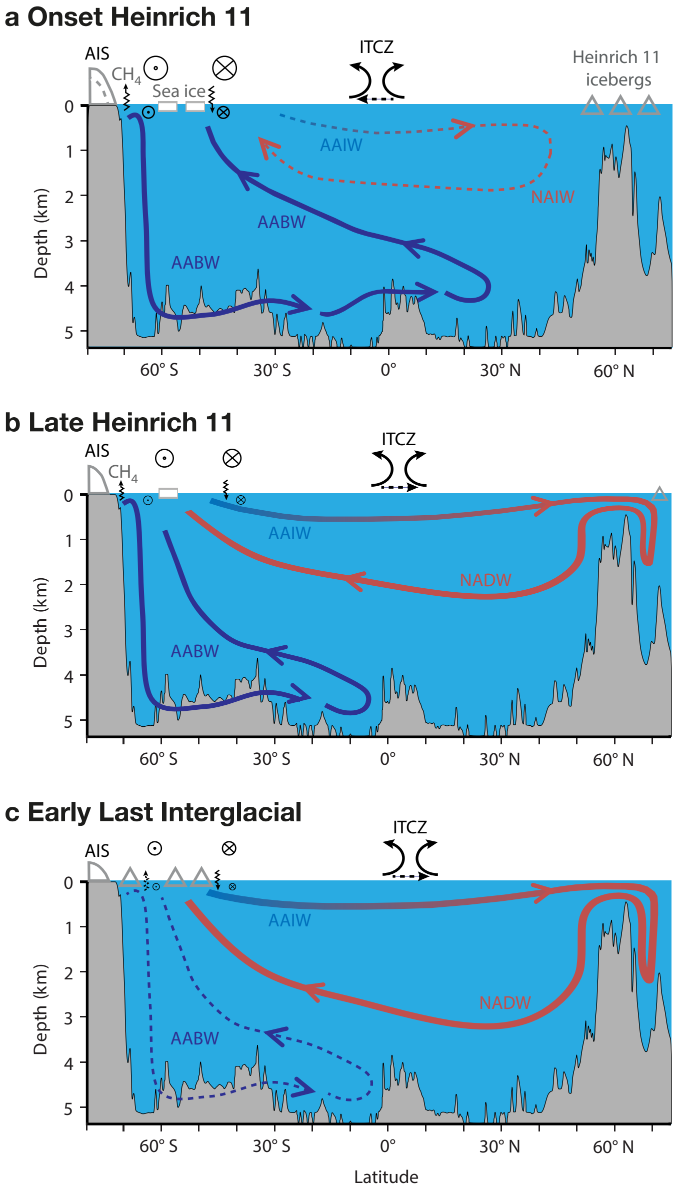

a Onset Heinrich 11
AIS
CH4
Sea ice
ITCZ
Heinrich 11 icebergs
AAIW
NAIW
AABW
AABW
Depth (km)
60° S
30° S
0°
30° N
60° N
b Late Heinrich 11
AIS
CH4
ITCZ
AAIW
NADW
AABW
Depth (km)
c Early Last Interglacial
AIS
ITCZ
AAIW
NADW
AABW
Depth (km)
Latitude

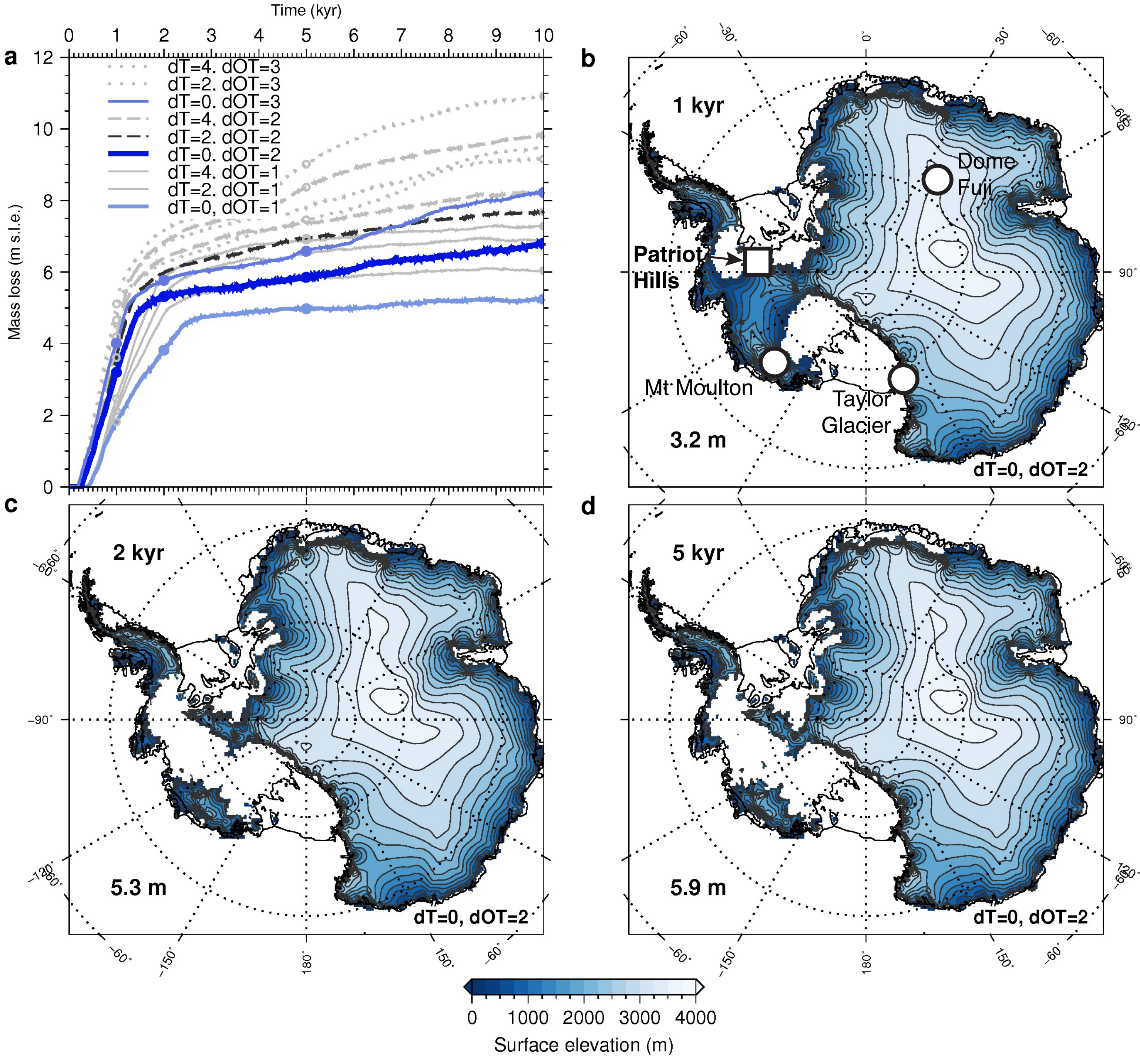

Time (kyr)
a
Mass loss (m s.l.e.)
dT=4, dOT=3
dT=2, dOT=3
dT=0, dOT=3
dT=4, dOT=2
dT=2, dOT=2
dT=0, dOT=2
dT=4, dOT=1
dT=2, dOT=1
dT=0, dOT=1
b
1 kyr
Dome Fuji
Patriot Hills
Mt Moulton
Taylor Glacier
3.2 m
dT=0, dOT=2
c
2 kyr
5.3 m
dT=0, dOT=2
d
5 kyr
5.9 m
dT=0, dOT=2
Surface elevation (m)
0
1000
2000
3000
4000

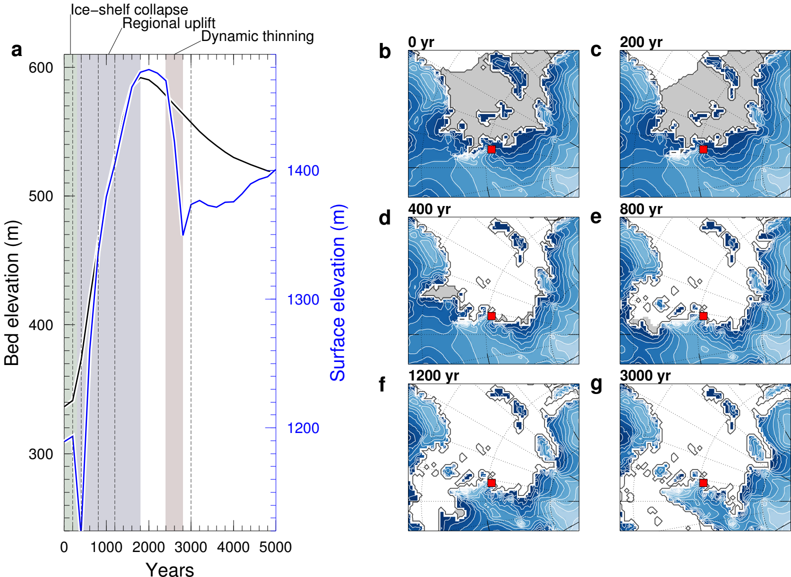
Ice−shelf collapse
Regional uplift
Dynamic thinning
a
Bed elevation (m)
Surface elevation (m)
Years
600
500
400
300
1400
1300
1200
0
1000
2000
3000
4000
5000
b
0 yr
c
200 yr
d
400 yr
e
800 yr
f
1200 yr
g
3000 yr